ACS APPLIED MATERIALS & INTERFACES

RESEARCH ARTICLE

www.acsami.org

Selective Deposition of CdSe Nanoparticles on Reduced Graphene Oxide to Understand Photoinduced Charge Transfer in Hybrid Nanostructures

Kehan Yu, Ganhua Lu, Shun Mao, Kehung Chen, Haejune Kim, Zhenhai Wen, and Junhong Chen*

Department of Mechanical Engineering, University of Wisconsin—Milwaukee, 3200 North Cramer Street, Milwaukee, Wisconsin 53211, United States

Supporting Information

ABSTRACT: A linker-free reduced graphene oxide (R-GO)-CdSe nanoparticle (CdSe NP) hybrid nanostructure was synthesized using a chemical vapor deposition method. CdSe NPs were selectively deposited on the surface of R-GO with controlled NP size and coverage. The distribution and morphology of CdSe NPs on R-GO were characterized by scanning electron microscopy, transmission electron microscopy, and atomic force microscopy. The resulting hybrid nanostructure exhibited photoresponse to both laser and simulated sunlight AM 1.5G excitation. The hybrid structure with low CdSe NP coverage showed distinct photoresponse times in air, N_2, NH_3, and NO_2, while high CdSe NP coverage led to nearly constant but three orders of magnitude smaller response time in all gases. Such a difference in photoresponse as a function of NP coverage is attributed to the energy band bending at the interface between the R-GO and the CdSe NP. The selective deposition of CdSe NPs on R-GO and the understanding of the subsequent photoinduced charge transfer can potentially lead to high-performance optoelectronic devices.

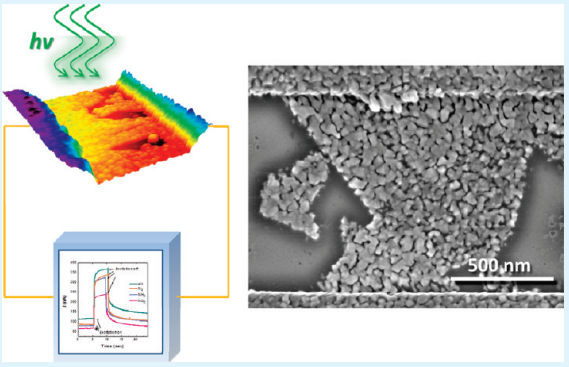

KEYWORDS: graphene, nanoparticle, hybrid nanostructure, selective deposition, charge transfer, photoresponse

INTRODUCTION

Graphene possesses many extraordinary properties and has become a subject of wide scientific interest in recent years.[1−14] Exceptionally high values have been reported for graphene: ballistic electron mobility,[15,16] thermal conductivity,[17] Young's modulus, fracture strength,[18] and specific surface area relevant to electrical energy storage.[9] Therefore, graphene holds great potential for numerous applications such as electronic devices, energy storage, solar cells, gas sensors, and photodetectors.[9,19−23] Unlike mechanical and vacuum-based preparation methods, obtaining graphene through chemically modified graphene oxide (GO) and reduced graphene oxide (R-GO) has been proved efficient, of low cost, and scalable.[24−26]

Semiconductor nanoparticles (NPs) are known for their size-dependent optical and electronic properties.[27,28] Combining semiconductor NPs with graphene points to a new direction in the design of optoelectronic devices such as solar cells and photodetectors with modulated performance. Prior studies have mainly focused on establishing synthetic strategies and characterizing resulting hybrid systems such as carbon nanotubes (CNTs) decorated with TiO_2,[29] SnO_2,[30] CdSe,[31,32] and CdS[33] nanocrystals. There are only a few reports on the synthesis of graphene-NP hybrid structures.[34−39] Moreover, most solution-based NP synthesis approaches require surface coating of NPs to prevent agglomeration. These organic coatings on NPs could limit conductivity and photoconductivity of NPs, thereby hindering widespread applications of NPs in optoelectronic devices.[40,41] Several groups have obtained R-GO-NP hybrid nanostructures using wet-chemical methods,[34−38] and much effort has been devoted to understanding the photoinduced charge transfer from semiconductor NPs to graphene. However, so far the charge transfer rate cannot be tuned for these hybrid nanostructures.

Here, we report on a facile fabrication of graphene-CdSe NP hybrids using a gas-phase chemical vapor deposition (CVD) method. CdSe NPs following their production can be selectively attached to graphene nanosheets without any chemical linkers. Upon visible light excitation, the R-GO-CdSe NP (G-NP) structure showed significantly faster photoresponse compared with the pure CdSe NP film. Moreover, the photoresponse amplitude and time can be modulated by the chemical environment and the NP coverage on R-GO. The results will help understand the transfer of photo-generated charge carriers in hybrid nanostructures, thus paving a way to practical applications of graphene and hybrid graphene-NP structures in optoelectronic devices.

RESULTS AND DISCUSSION

G-NP photodetectors were fabricated by drop casting R-GO on interdigitated gold electrodes and the subsequent CdSe NP

Received: April 20, 2011
Accepted: June 8, 2011
Published: June 08, 2011

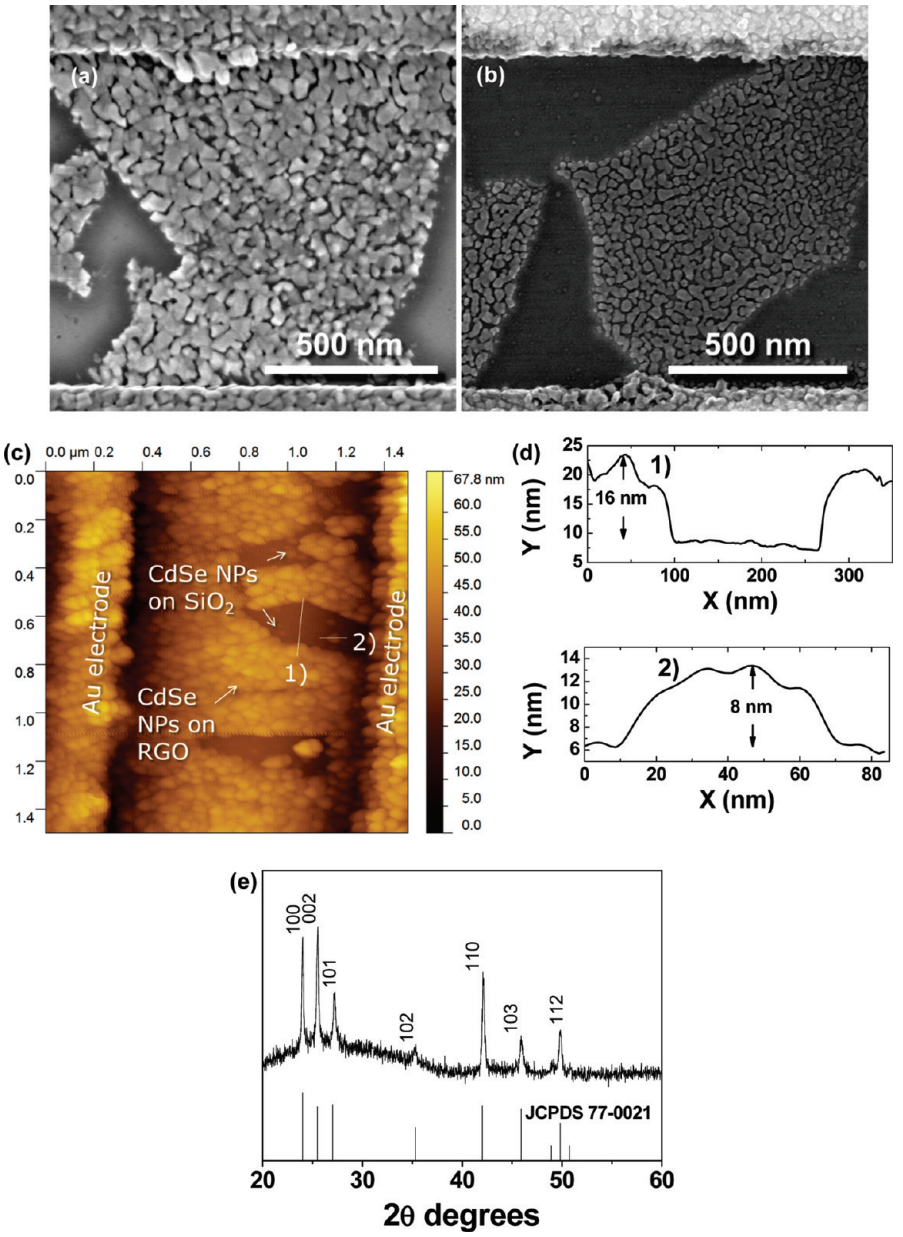

Figure 1. SEM images of (a) a G-*h*NP photodetector and (b) a G-*l*NP photodetector. (c) AFM images of a G-*h*NP photodetector. (d) Height profiles taken along white lines labeled as 1) and 2) in panel c. (e) XRD 2θ scan of the CdSe NPs. The standard XRD pattern (JCPDS card #77-0021) for CdSe is also indicated.

assembly using CVD. The CVD process took place without catalysts at 500 °C and atmospheric pressure. Parallel Au electrodes with spacings of 1 μm were fabricated by an e-beam lithography process on silicon wafers with a 300 nm thick SiO_2 dielectric layer.[42] The CVD technique for coating CdSe NPs is facile, and graphene nanosheets can be fully covered with CdSe NPs typically within 1 min. The NP coverage and the NP size are tunable through varying the deposition duration.

Figure 1a and b shows scanning electron microscopy (SEM) images of the G-NP photodetectors with different levels of NP coverage. Figure 1a shows a high-coverage G-NP (G-*h*NP) photodetector with CdSe deposition for 40 s, while a low-coverage G-NP (G-*l*NP) photodetector with CdSe deposition for 20 s is shown in Figure 1b. The NP sizes can be estimated according to the SEM images. Smaller NPs shown in Figure 1b (20 s growth) had a lateral size of about 10 nm. Then they grew to 30−60 nm in the next 20 s. With increasing deposition time, NPs were more and more densely packed on the graphene sheets. The CdSe NPs grew on gold electrodes as well since gold can catalyze the growth of CdSe NPs.[43,44] It is evident that the profile of the underlying R-GO sheet is outlined by the attached NPs. In other words, CdSe NPs preferentially attached to the surface of R-GO sheets. Only sparse CdSe NPs (dark dots with lighter outlines) can be barely identified on the SiO_2 substrate due to the charging effect (Figure 1a and b). The atomic force microscopy (AFM) image shows a small area in the G-*h*NP photodetector (Figure 1c). A height profile plot shows that the height of CdSe NPs is about 16 nm (profile 1, Figure 1d). Meanwhile, an individual NP lying on the SiO_2 substrate is about 8 nm high as shown by the height profile plot (profile 2, Figure 1d).

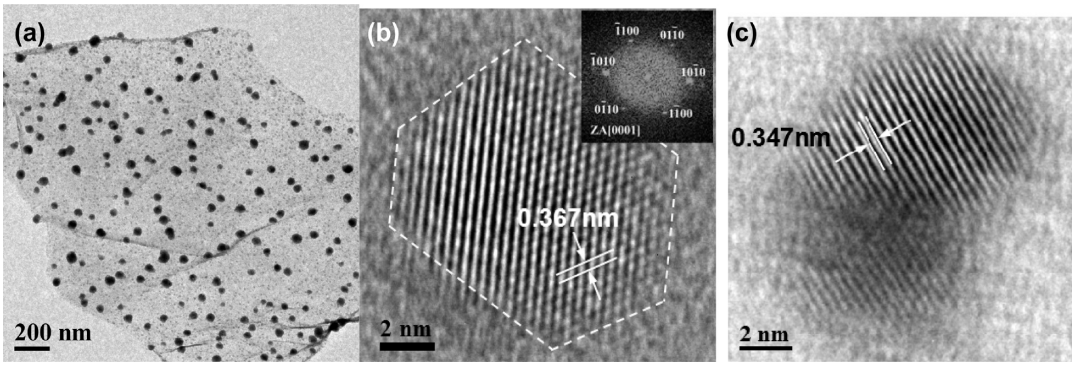

Figure 2. (a) TEM image of G-NP with 30-s CdSe NP deposition. (b) HRTEM image of an individual CdSe NP decorated on graphene and observed along the [0001] direction. The inset shows the corresponding diffractogram of the CdSe NP. (c) HRTEM image of an individual CdSe NP decorated on graphene and observed perpendicular to the [0001] direction.

This suggests that the CdSe of the G-*h*NP is probably a double-layer NP film. Interestingly, the NPs are flat rather than spherical with their lateral sizes (~60 nm) much greater than their heights (~8 nm). The X-ray diffraction (XRD) spectrum of the CdSe NPs is shown in Figure 1e, indicating that the CdSe NPs are of wurtzite (WZ) structure (JCPDS card #77-0021).

The structure of the G-NP was further investigated by transmission electron microscopy (TEM) and high resolution TEM (HRTEM). Figure 2a is a TEM image of an R-GO platelet decorated with CdSe NPs deposited for 30 s. Sparse larger CdSe NPs (20−30 nm) along with a great number of smaller NPs (5−6 nm) can be seen on the graphene surface. The size difference may be related to the cooling process at the end of the CVD synthesis. Smaller NPs were formed in the cooling process when a lower temperature decelerated the chemical reaction. Figure 2b is an HRTEM image of an individual CdSe NP on the graphene. A dashed line outlines the hexagonal shape of the NP. The lattice spacing analysis by the numerical diffractogram (the inset of Figure 2b) reveals that the orientation of the NP is along the [0001] direction. The measured lattice spacing of 0.367 nm corresponds to the $(10\bar{1}0)$ plane of CdSe. Another individual NP on the graphene was observed in a direction perpendicular to [0001] shown in an HRTEM image of Figure 2c. The lattice spacing of 0.347 nm can be indexed as the (0002) plane of CdSe. The WZ (hexagonal) structure of the CdSe is consistent with the XRD 2θ scan shown in Figure 1d.

The selective deposition was reported for CdSe NPs on CNTs.[45,46] Investigation revealed that the hexagonal (0001) planes of CdSe nanocrystal match the sp^2 carbon lattice epitaxially.[45] Besides the CNTs, CdSe NPs can also be attached on graphene (sp^2 carbon) rather than on glassy carbon or diamond (sp^3 carbon).[46] Another group reported that CdSe NPs were connected with R-GO through nonpolar facets instead of polar facets, i. e., (0001).[38] Like CNTs and pure graphene, R-GO mainly consists of sp^2 carbon. However, the surface of R-GO is still decorated with some oxygen functional groups,[26] as evidenced by the presence of −OH and −COOH in the X-ray photoelectron spectroscopy (XPS) spectrum (Figure S2, Supporting Information). The oxygen functional groups could readily anchor Cd atoms of CdSe NPs. The HRTEM image confirms that both polar and nonpolar facets of CdSe NPs can indeed attach to the graphene basal plane (Figure 2b and c). Although some of the structural features of the R-GO, such as its convoluted/bent morphology, may be detrimental for NP anchoring, the overall planar feature of R-GO makes it more efficient for NP attachment compared with the curved CNT surface.

The photoinduced charge transfer from CdSe NPs to R-GO was evidenced by monitoring the current change of a photodetector under illumination (Figure 3). In order to maximize the light absorption and charge transfer, the R-GO on an interdigitated electrode was deposited with CdSe NPs for as long as 5 min until its surface was fully covered with NPs (inset of Figure 3a). The current through the device with and without simulated sunlight irradiation (AM 1.5 G, 100 mW cm^{-2}) was monitored with a constant bias voltage of 0.01 V. Figure 3a shows that the photosensitivity, defined as the ratio of the current change ($I_{ex} - I_{dark}$) under the irradiation to that in the dark (I_{dark}), of the G-*h*NP photodetector can be as high as 230% (in air). The photodetector exhibited a fast photoresponse as well. The left portion of the curve corresponding to the current increase was fitted exponentially, and the response time constant is estimated as 8.5 ms.

The efficient transfer of photoinduced charge carriers from CdSe NPs to R-GO has been reported by a few groups.[35,38,47] However, the reported photosensitivities varied from ~10%[35] to ~1,600%,[38] with the best response time (250 μs)[38] being much faster than the rest. One possible reason for such discrepancies was that the light source, including the power and the wavelength, used to excite the photodetectors varied from one to another. However, the real mechanism behind such variation remains unclear so far. Considering the high charge carrier mobility of graphene and the ultrafast energy transfer rate from QDs to graphene,[37,47] the electronic coupling at the interface between R-GO and NPs may play a key role in the response time. Therefore, we intentionally immersed the G-*h*NP photodetector in different gaseous environments and investigated the modulation of photoresponse.

Figure 3b shows the photoresponse of the G-*h*NP device under 532-nm laser excitation (50 mW) in air, N_2, NH_3 (1%), and NO_2 (100 ppm) at room temperature. The response times were 8.7 ms, 6.9 ms, 7.6 ms, and 8.3 ms in air, N_2, NH_3, and NO_2, respectively. These response times are quite similar. As a result of high coverage of CdSe NPs, the NP/graphene interface was not extensively exposed to the surrounding gaseous environment. Therefore, neither inert nor redox gases could affect the response time significantly. We also note that the dark current (current before excitation) shifted in different gases (Figure 3b).

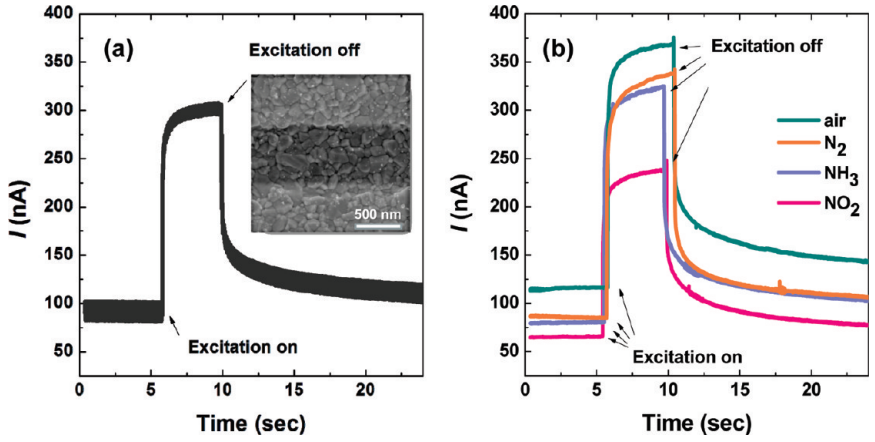

Figure 3. Photoinduced current response versus time of a G-*h*NP photodetector under irradiation of (a) simulated sunlight 100 mW cm^{-2} (AM 1.5 G) in air and (b) 532-nm laser of ~50 mW with different gas flows of air, N_2, NH_3, and NO_2. The inset of panel a is an SEM image of the corresponding device. All current changes were recorded with a bias voltage of 0.01 V.

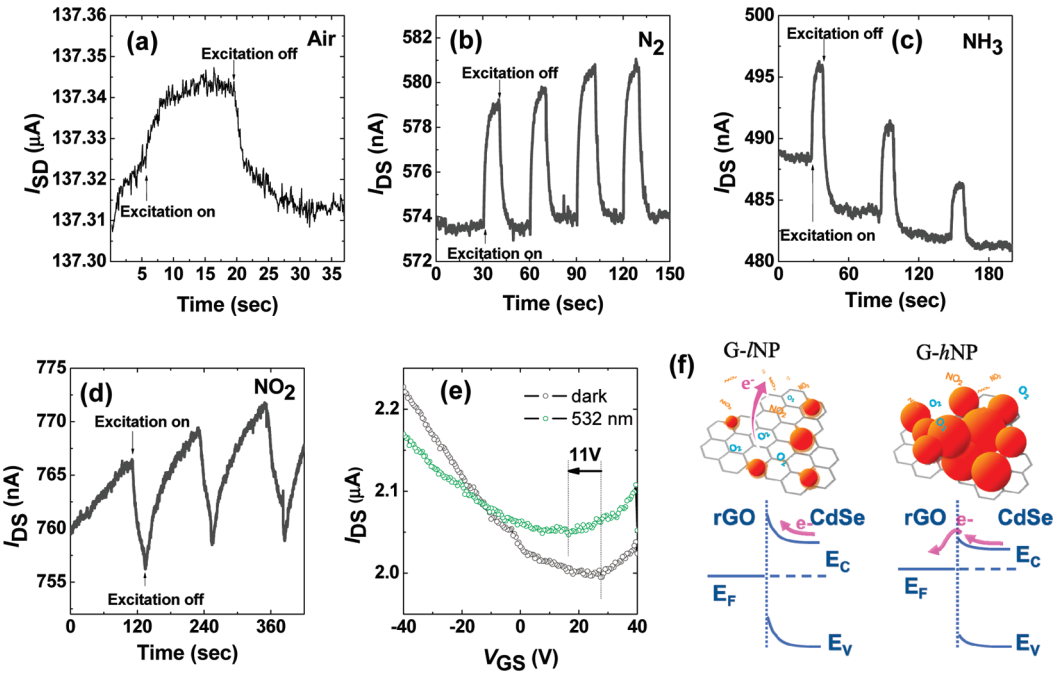

Figure 4. Photoinduced current response versus time of a G-*l*NP photodetector under chopped irradiation of a 532-nm laser of ~50 mW in different gases (a) air, (b) N_2, (c) NH_3, and (d) NO_2. All current changes were recorded under a bias voltage of 0.01 V. (e) Drain-source current versus back gate voltage of a PMMA-coated G-*l*NP photodetector with and without laser irradiation. The drain-source bias voltage was 0.1 V. (f) Energy band bending caused by gases at the interface between CdSe NPs and R-GO of G-*l*NP and G-*h*NP photodetectors.

The G-*h*NP photodetector was exposed to air, NO_2, NH_3, and N_2, sequentially. The electrons in n-type CdSe were first extracted by NO_2 (electron acceptor), resulting in a decrease in the dark current. Then, before complete desorption of NO_2, electrons were enriched by NH_3 (electron donor), resulting in an increase in the dark current. Finally, the dark current recovered slowly in N_2 flow to the level close to that in air. We assume that in this case the R-GO sheets were completely covered by NPs and exposure of the p-type R-GO to the gaseous environment was limited. Otherwise, the dark current would have changed in an opposite direction if the p-type R-GO was also modulated by gas exposure.

For comparison, a G-*l*NP photodetector was excited in air, NO_2, NH_3, and N_2 under the same condition. This device was deposited with CdSe NPs for 20 s. Figure 4 shows the current change upon light excitation in different gas flows. The response times were 2.24 s, 1.61 s, 1.29 s, and 9.28 s in air, N_2, NH_3, and NO_2 at room temperature, respectively. Not only was the photoresponse about 2 orders of magnitude slower than that of the G-*h*NP, but also the photosensitivities were below 2% (two orders of magnitude lower!). Because of fewer NPs on R-GO, the lower photosensitivity is a result of less photoinduced charge transfer. Interestingly, this device showed an opposite trend: the current decreased rather than increasing upon laser illumination in the NO_2 flow (Figure 4d). Because of the low coverage of NPs on the graphene sheet, the graphene would be extensively exposed to the ambient. The R-GO is well-known for gas sensing

performance based on adsorption/desorption of redox gaseous molecules.[48−50] Particularly, NO_2 is a strong oxidizer with electron withdrawing power; therefore, its adsorption on the R-GO surface would lead to enriched holes in R-GO. For the G-*l*NP, NO_2 can extract electrons through the exposed portion of the R-GO. The photoinduced electrons transferred from the CdSe NPs would recombine with holes in the R-GO, thereby downgrading the hole concentration in the R-GO and leading to a decreased current response (Figure 4d). For the G-*h*NP, there was only limited contact between NO_2 and R-GO, and the adsorption of NO_2 on G-*h*NP was negligible. Therefore, the photoinduced electron transfer from CdSe NPs to R-GO still dominated, which led to an increased current response. The photoinduced electron transfer was further confirmed by measuring the transfer characteristic of a G-*l*NP FET. The G-*l*NP FET was spin-coated with a poly(methyl methacrylate) (PMMA) thin film in order to avoid the ambient gas exposure. The Dirac point (lowest point of the FET curve) down shifted by about 11 V under laser irradiation (Figure 4e). This reflected an increased electron concentration in the FET channel, which was injected from the excited CdSe NPs.

A likely mechanism for the photoresponse time modulation is the presence of adsorbed O_2 or NO_2 on the R-GO, which leads to electron removal and upward bending of energy bands of CdSe NPs at the interface, thereby increasing the injection barrier (Figure 4f, left panel). The Fermi level of R-GO (+0.38 to +0.88 V vs the standard hydrogen electrode, SHE) is well below the bottom edge of the conduction band of CdSe (≤ -1.0 V vs SHE).[51−53] Decreasing CdSe NP sizes increases the driving force for charge injection as it shifts the conduction band to a more-negative potential. The injection barrier of the G-*l*NP devices would slow the charge transfer rate. The response time of NO_2 > air > N_2 > NH_3 is a result of the relative ability of oxidization of NO_2 (100 ppm in air) > O_2 in air > N_2 > NH_3 (1% in air). The upward band bending is not supposed to occur in N_2 and NH_3. However, the G-*l*NP devices were pre-exposed to air after the CVD process and before the photoexcitation experiment. By no means can the adsorbed oxygen desorb at room temperature in a short period of time. A wise way to minimize the upward bending is thus to fully seal the graphene in the CVD process with CdSe NPs before the air exposure. Indeed, the NP layer prevented the R-GO from gas exposure for the G-*h*NP. Therefore, the response times of the G-*h*NP photodetector in air and NO_2 were only slightly greater than those in N_2 and NH_3. The photoresponse of the G-*h*NP in ms scale indicated a negligible band bending in different chemical gases (Figure 4f, right panel). The role of the adsorbed oxygen on R-GO was further investigated with a G-*l*NP photodetector sealed with PMMA after CVD. As shown in Figure S3 in the Supporting Information, the response time was 2.07 s, similar to those in various gas flows without PMMA. Again, it shows that a short exposure in air will lead to a long-term adsorption of oxygen, although the PMMA can block the device form further exposure to air.

Hou et al. highlighted that good adhesion or stability of the CdSe NPs on R-GO was another possible way to facilitate the charge transfer.[38] The CdSe NPs can be scratched off with a blade from the G-*l*NP device deposited for 20 s. But the G-*h*NP device showed much better stability against scratching. With good contact, the photoinduced electrons and holes will transfer to the R-GO separately and then drift to opposite electrodes of the device by the external electric field.[20] However, a poor contact will hinder the hole transfer, and the accumulated holes left in NPs will prolong the response to more than hundreds of seconds by a gate effect.[54−56]

Furthermore, the photoresponse time of the CdSe itself was not affected by redox gases. As a control, a pure CdSe NP photodetector was fabricated with 5-min CdSe NP deposition and then tested in different gas flows under illumination. The response times were 32.5 ms, 42.5 ms, 32.6 ms, and 35.4 ms in air, N_2, NH_3, and NO_2 at room temperature under 532-nm laser excitation (50 mW), respectively (Figure S4a, Supporting Information). A response time of 37.8 ms was obtained with stimulated sunlight (AM1.5G 100 mW cm^{-2}) illumination in air (Figure S4b, Supporting Information). Obviously, the response times of the pure CdSe device are longer than those of the G-*h*NP devices. The high charge carrier mobility of graphene facilitated the transport of injected charge carriers in a G-NP photodetector. But the charge carriers will have to move across many grain boundaries within the pure polycrystalline CdSe film (Figure S4c, Supporting Information). It is worth noting that all response times of G-*h*NP devices were almost the same regardless the type of gases exposed. Although redox gases will change the conductivity of the pure CdSe film (Figure S4d, Supporting Information), the charge transfer rate is mainly controlled by the physics at the CdSe/R-GO interface.

CONCLUSIONS

We have demonstrated selective deposition of CdSe NPs on R-GO using a catalyst-free CVD method. The coverage level of NPs on R-GO can be controlled by CVD duration. Compared with pure CdSe NPs and G-*l*NP, the G-*h*NP photodetector possessed much faster photoresponse. The response time of a G-*l*NP photodetector can be modulated by different gas exposures. This behavior can be interpreted by the energy band bending of CdSe at the R-GO/NP interface due to gas adsorption. To the best of our knowledge, this is the first report on manipulation of the photoresponse time of graphene−semiconductor nanohybrids. The ability to control the photoinduced charge transfer demonstrated in this study suggests that the G-NP hybrid structure and the catalyst-free CVD fabrication process are promising for optoelectronic device applications. For instance, results presented in this study have important implications for graphene−NP solar cells. In a photoelectrochemical solar cell, the electrolyte contains strong redox species. If the graphene is directly in contact with the electrolyte, the charge separation at the graphene−NP interface will be hindered because of the energy band bending. Therefore, a densely packed structure like the G-*h*NP demonstrated in this work is desired for a high-efficiency photoelectrochemical solar cell.

MATERIALS AND METHODS

Chemicals. Cadmium shot (99.9999%) and selenium shot (99.999%) were purchased from Alfa Aesar. Natural graphite (SP-1) was purchased from Bay Carbon, MI.

Synthesis of the G-CdSe Hybrid Nanomaterials. GO was synthesized using a modified Hummers method.[57] To obtain R-GO, GO suspension in water was dispersed on substrates of interest (such as metal electrodes and TEM grids) by drop casting. Gold interdigitated electrodes[42] with a finger width and an interfinger spacing of about 1 μm were fabricated by an e-beam lithography process and used as the FET substrates. After drying in air, the GO on substrates was converted to R-GO by annealing in Ar flow at 500 °C for 1 h. The R-GO was significantly more conductive than GO.

CdSe NPs were synthesized using CVD at 500 °C and atmospheric pressure in a tube furnace. High-purity Cd and Se were used as source materials. The Cd metal source was fixed in a graphite crucible and placed inside a quartz tube in the middle of the tube furnace. The Se source was placed in another graphite crucible upstream (close to the end of the tube furnace) where the temperature was 350 °C. The R-GO on substrates used to collect CdSe NPs was located at the downstream of precursor sources. A flow of Ar (99.99 %, 1 lpm) was used as the carrier gas. A schematic of the experimental setup is illustrated in Supporting Information, Figure S1.

A thin film of CdSe NPs can be coated onto the substrate with a simple three-step process: (1) preheat the substrate and the Cd source by moving the CVD reactor to a position so that the Se was outside the furnace; (2) insert the whole quartz tube into the furnace so that the temperature of the Se source is approximately 350 °C; (3) after the intended duration (20 s−5 min), cool down the Se source by withdrawing the reactor so that the Se was outside the furnace. The CVD process ends with cooling the whole reactor at room temperature. After the CVD process, dark-brown products were observed on a wide surface area of the substrate and the inner wall of the quartz tube.

Characterization. SEM was conducted on a HITACHI S-4800 at an accelerating voltage of 2 kV. TEM analysis was carried out using a Hitachi H 9000 NAR TEM with a point resolution of 0.18 nm at 300 kV in the phase contrast HRTEM imaging mode. XRD was conducted with a Scintag XDS 2000 X-ray diffractometer. AFM was conducted with an Agilent Technology 5420 AFM with a cantilever (Nanosensors PPP-NCH). Electrical measurements were performed at room temperature using a Keithley 2602 source meter. The laser source used in the photoresponse measurement was 532 nm in wavelength and 50 mW in power. A Newport 94021A simulated sunlight source was used for the photoresponse measurement with filter (Newport 81088A).

■ ASSOCIATED CONTENT

Ⓢ Supporting Information. Experimental setup for CVD synthesis of G-NP hybrid structures; C1s XPS spectra of R-GO obtained by thermal annealing; photoresponse of the G-*l*NP photodetector covered with PMMA; photoresponse and gas sensing properties of pure CdSe NP films; and charge transfer processes within the pure polycrystalline CdSe film and G-NP structure. This material is available free of charge via the Internet at http://pubs.acs.org.

■ AUTHOR INFORMATION

Corresponding Author
*E-mail: jhchen@uwm.edu.

■ ACKNOWLEDGMENT

This work was financially supported by the NSF (CMMI-0900509), the US DOE (DE-EE0003208), and We Energies. TEM and SEM analyses were performed in the UWM HRTEM Laboratory and UWM Electron Microscope Laboratory, respectively. AFM and XRD were conducted at the AAF of UWM. We thank M. Gajdardziska-Josifovska for providing TEM access, D. Robertson for technical support with TEM, S. E. Hardcastle for technical support with AFM and XRD, and L. E. Ocola for assistance in the electrode fabrication. The interdigitated electrodes were fabricated at the Center for Nanoscale Materials of Argonne National Laboratory, which is supported by the U.S. Department of Energy, Office of Science, Office of Basic Energy Sciences, under Contract No. DE-AC02-06CH11357.

■ REFERENCES

(1) Li, X.; Cai, W.; An, J.; Kim, S.; Nah, J.; Yang, D.; Piner, R.; Velamakanni, A.; Jung, I.; Tutuc, E.; Banerjee, S. K.; Colombo, L.; Ruoff, R. S. *Science* **2009**, *324*, 1312.
(2) Berger, C.; Song, Z.; Li, X.; Wu, X.; Brown, N.; Naud, C.; Mayou, D.; Li, T.; Hass, J.; Marchenkov, A. N.; Conrad, E. H.; First, P. N.; de Heer, W. A. *Science* **2006**, *312*, 1191.
(3) Novoselov, K. S.; Geim, A. K.; Morozov, S. V.; Jiang, D.; Katsnelson, M. I.; Grigorieva, I. V.; Dubonos, S. V.; Firsov, A. A. *Nature* **2005**, *438*, 197.
(4) Novoselov, K. S.; Jiang, D.; Schedin, F.; Booth, T. J.; Khotkevich, V. V.; Morozov, S. V.; Geim, A. K. *Proc. Natl. Acad. Sci. U.S.A.* **2005**, *102*, 10451.
(5) Novoselov, K. S.; Geim, A. K.; Morozov, S. V.; Jiang, D.; Zhang, Y.; Dubonos, S. V.; Grigorieva, I. V.; Firsov, A. A. *Science* **2004**, *306*, 666.
(6) Meyer, J. C.; Geim, A. K.; Katsnelson, M. I.; Novoselov, K. S.; Booth, T. J.; Roth, S. *Nature* **2007**, *446*, 60.
(7) Ferrari, A. C.; Meyer, J. C.; Scardaci, V.; Casiraghi, C.; Lazzeri, M.; Mauri, F.; Piscanec, S.; Jiang, D.; Novoselov, K. S.; Roth, S.; Geim, A. K. *Phys. Rev. Lett.* **2006**, *97*, 187401.
(8) Li, X.; Zhu, Y.; Cai, W.; Borysiak, M.; Han, B.; Chen, D.; Piner, R. D.; Colombo, L.; Ruoff, R. S. *Nano Lett.* **2009**, *9*, 4359.
(9) Stoller, M. D.; Park, S.; Zhu, Y.; An, J.; Ruoff, R. S. *Nano Lett.* **2008**, *8*, 3498.
(10) Novoselov, K. S.; McCann, E.; Morozov, S. V.; Fal'ko, V. I.; Katsnelson, M. I.; Zeitler, U.; Jiang, D.; Schedin, F.; Geim, A. K. *Nat. Phys.* **2006**, *2*, 177.
(11) Stankovich, S.; Dikin, D. A.; Dommett, G. H. B.; Kohlhaas, K. M.; Zimney, E. J.; Stach, E. A.; Piner, R. D.; Nguyen, S. T.; Ruoff, R. S. *Nature* **2006**, *442*, 282.
(12) Cai, W.; Zhu, Y.; Li, X.; Piner, R. D.; Ruoff, R. S. *Appl. Phys. Lett.* **2009**, *95*, 123115.
(13) Dreyer, D. R.; Ruoff, R. S.; Bielawski, C. W. *Angew. Chem., Int. Ed.* **2010**, *49*, 9336.
(14) Potts, J. R.; Dreyer, D. R.; Bielawski, C. W.; Ruoff, R. S. *Polymer* **2010**, *52*, 5.
(15) Chen, J.-H.; Jang, C.; Xiao, S.; Ishigami, M.; Fuhrer, M. S. *Nat. Nanotechnol.* **2008**, *3*, 206.
(16) Bolotin, K. I.; Sikes, K. J.; Jiang, Z.; Klima, M.; Fudenberg, G.; Hone, J.; Kim, P.; Stormer, H. L. *Solid State Commun.* **2008**, *146*, 351.
(17) Balandin, A. A.; Ghosh, S.; Bao, W.; Calizo, I.; Teweldebrhan, D.; Miao, F.; Lau, C. N. *Nano Lett.* **2008**, *8*, 902.
(18) Lee, C.; Wei, X.; Kysar, J. W.; Hone, J. *Science* **2008**, *321*, 385.
(19) Schedin, F.; Geim, A. K.; Morozov, S. V.; Hill, E. W.; Blake, P.; Katsnelson, M. I.; Novoselov, K. S. *Nat. Mater.* **2007**, *6*, 652.
(20) Xia, F.; Mueller, T.; Lin, Y.-m.; Valdes-Garcia, A.; Avouris, P. *Nat. Nanotechnol.* **2009**, *4*, 839.
(21) Wang, X.; Ouyang, Y.; Li, X.; Wang, H.; Guo, J.; Dai, H. *Phys. Rev. Lett.* **2008**, *100*, 206803.
(22) Blake, P.; Brimicombe, P. D.; Nair, R. R.; Booth, T. J.; Jiang, D.; Schedin, F.; Ponomarenko, L. A.; Morozov, S. V.; Gleeson, H. F.; Hill, E. W.; Geim, A. K.; Novoselov, K. S. *Nano Lett.* **2008**, *8*, 1704.
(23) Wang, X.; Zhi, L.; Mullen, K. *Nano Lett.* **2007**, *8*, 323.
(24) Li, D.; Muller, M. B.; Gilje, S.; Kaner, R. B.; Wallace, G. G. *Nat. Nanotechnol.* **2008**, *3*, 101.
(25) Eda, G.; Fanchini, G.; Chhowalla, M. *Nat. Nanotechnol.* **2008**, *3*, 270.
(26) Dreyer, D. R.; Park, S.; Bielawski, C. W.; Ruoff, R. S. *Chem. Soc. Rev.* **2010**, *39*, 228.
(27) Alivisatos, A. P. *J. Phys. Chem.* **1996**, *100*, 13226.
(28) Murray, C. B.; Norris, D. J.; Bawendi, M. G. *J. Am. Chem. Soc.* **1993**, *115*, 8706.
(29) Banerjee, S.; Wong, S. S. *Nano Lett.* **2002**, *2*, 195.
(30) Han, W. Q.; Zettl, A. *Nano Lett.* **2003**, *3*, 681.
(31) Banerjee, S.; Wong, S. S. *Chem. Commun* **2004**, 1866.
(32) Haremza, J. M.; Hahn, M. A.; Krauss, T. D. *Nano Lett.* **2002**, *2*, 1253.

(33) Shi, J. H.; Qin, Y. J.; Wu, W.; Li, X. L.; Guo, Z. X.; Zhu, D. B. *Carbon* **2004**, *42*, 455.
(34) Williams, G.; Seger, B.; Kamat, P. V. *ACS Nano* **2008**, *2*, 1487.
(35) Geng, X.; Niu, L.; Xing, Z.; Song, R.; Liu, G.; Sun, M.; Cheng, G.; Zhong, H.; Liu, Z.; Zhang, Z.; Sun, L.; Xu, H.; Lu, L.; Liu, L. *Adv. Mater.* **2010**, *22*, 638.
(36) Williams, G.; Kamat, P. V. *Langmuir* **2009**, *25*, 13869.
(37) Cao, A.; Liu, Z.; Chu, S.; Wu, M.; Ye, Z.; Cai, Z.; Chang, Y.; Wang, S.; Gong, Q.; Liu, Y. *Adv. Mater.* **2009**, *22*, 103.
(38) Lin, Y.; Zhang, K.; Chen, W.; Liu, Y.; Geng, Z.; Zeng, J.; Pan, N.; Yan, L.; Wang, X.; Hou, J. G. *ACS Nano* **2010**, *4*, 3033.
(39) Lu, G.; Mao, S.; Park, S.; Ruoff, R.; Chen, J. *Nano Res.* **2009**, *2*, 192.
(40) Jarosz, M. V.; Porter, V. J.; Fisher, B. R.; Kastner, M. A.; Bawendi, M. G. *Phys. Rev. B* **2004**, *70*, 195327.
(41) Morgan, N. Y.; Leatherdale, C. A.; Drndicacute, M.; Jarosz, M. V.; Kastner, M. A.; Bawendi, M. *Phys. Rev. B* **2002**, *66*, 075339.
(42) Lu, G. H.; Ocola, L. E.; Chen, J. H. *Adv. Mater.* **2009**, *21*, 2487.
(43) Venugopal, R.; Lin, P.-I.; Liu, C.-C.; Chen, Y.-T. *J. Am. Chem. Soc.* **2005**, *127*, 11262.
(44) Zhang, Y. F.; You, L. P.; Shan, X. D.; Wei, X. L.; Huo, H. B.; Xu, W. J.; Dai, L. *J. Phys. Chem. C* **2007**, *111*, 14343.
(45) Hungría, A.; Juárez, B.; Klinke, C.; Weller, H.; Midgley, P. *Nano Res.* **2008**, *1*, 89.
(46) Juarez, B. H.; Meyns, M.; Chanaewa, A.; Cai, Y.; Klinke, C.; Weller, H. *J. Am. Chem. Soc.* **2008**, *130*, 15282.
(47) Chen, Z.; Berciaud, S.; Nuckolls, C.; Heinz, T. F.; Brus, L. E. *ACS Nano* **2010**, *4*, 2964.
(48) Lu, G.; Ocola, L. E.; Chen, J. *Nanotechnol.* **2009**, *20*, 445502.
(49) Lu, G.; Ocola, L. E.; Chen, J. *Appl. Phys. Lett.* **2009**, *94*, 083111.
(50) Lu, G.; Park, S.; Yu, K.; Ruoff, R. S.; Ocola, L. E.; Rosenmann, D.; Chen, J. *ACS Nano* **2011**, *5*, 1154.
(51) Kong, B.-S.; Geng, J.; Jung, H.-T. *Chem. Commun.* **2009**, 2174.
(52) Becerril, H. A.; Stoltenberg, R. M.; Tang, M. L.; Roberts, M. E.; Liu, Z.; Chen, Y.; Kim, D. H.; Lee, B.-L.; Lee, S.; Bao, Z. *ACS Nano* **2010**, *4*, 6343.
(53) Robel, I.; Subramanian, V.; Kuno, M.; Kamat, P. V. *J. Am. Chem. Soc.* **2006**, *128*, 2385.
(54) Li, X.; Jia, Y.; Cao, A. *ACS Nano* **2009**, *4*, 506.
(55) Juarez, B. H.; Klinke, C.; Kornowski, A.; Weller, H. *Nano Lett.* **2007**, *7*, 3564.
(56) Biebersdorf, A.; Dietmuller, R.; Susha, A. S.; Rogach, A. L.; Poznyak, S. K.; Talapin, D. V.; Weller, H.; Klar, T. A.; Feldmann, J. *Nano Lett.* **2006**, *6*, 1559.
(57) Hummers, W. S.; Offeman, R. E. *J. Am. Chem. Soc.* **1958**, *80*, 1339.